RESEARCH REPORT

VTT-R-00972-22

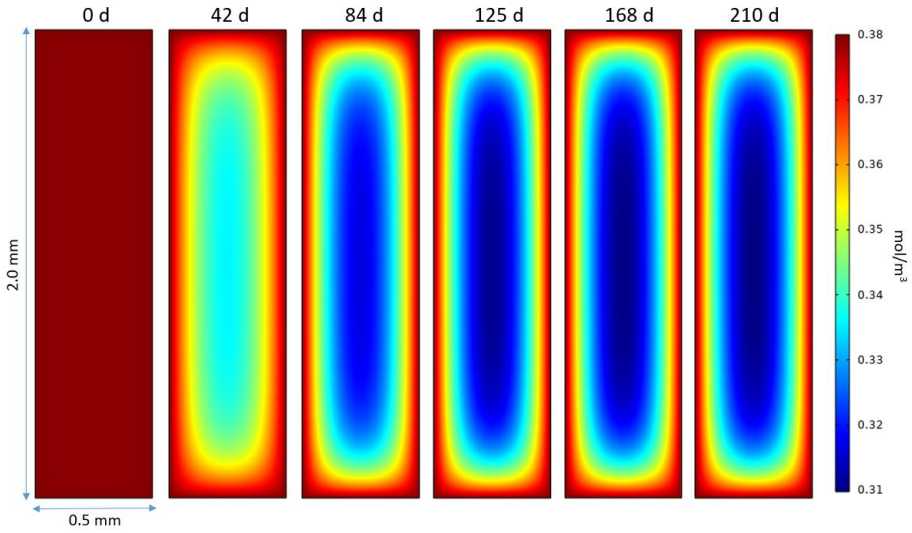

A finite-element model for antioxidant consumption

Authors: Jukka Vaari

Confidentiality: Restricted to SAFIR2022 until 1.12.2025

Version: 28.11.2022

VTT

beyond the obvious

Report's title A finite-element model for antioxidant consumption	
Customer, contact person, address SAFIR2022	**Order reference**
Project name SAFIR2022_SAMPO 2022	**Project number/Short name** 131813/SAMPO
Author(s) Jukka Vaari	**Pages** 21/
Keywords Polyethylene, antioxidant consumption, finite-element modelling	**Report identification code** VTT-R-00972-22

Summary

The main stressors causing aging in polymeric materials are temperature, radiation and presence of oxygen. To mitigate aging effects, antioxidants are normally added to the polymer composition. Antioxidant levels in materials can offer an early clue into the time available before materials start to severely degrade. Monitoring the antioxidant level is possible using e.g. DSC or FTIR. A complementary approach to experiments is offered by numerical methods to estimate antioxidant consumption.

In this work, we have initiated the development of numerical antioxidant consumption modelling beyond the state of the art. The polymer degradation mechanism, oxygen diffusion, and antioxidant depletion were implemented in both 2D and 3D finite-element models to obtain realistic component-scale predictions on thermal degradation. As a novelty, antioxidant diffusion and evaporation models were added.

The capabilities of the model were demonstrated by simulating a radiothermal (T=47 ºC, dose rate 77.8 Gy/h) aging of silane-crosslinked, 0.5 mm thick polyethylene up to 210 days. It was shown that the model can reproduce experimentally observed levels of hydroperoxide and carbonyl species, and predict a decrease of the molecular weight of the material such that the cross-linked gel network is completely degraded, and that the mechanical properties of the material are severely compromised.

Confidentiality	Restricted to SAFIR2022 until 1.12.2025

Espoo 16.12.2022

Written by	**Reviewed by**
Jukka Vaari Senior Scientist	Konsta Sipilä Senior Scientist

VTT's contact address

Distribution (customer and VTT)

VTT Archive

Approval

VTT TECHNICAL RESEARCH CENTRE OF FINLAND LTD

Date:	
Signature:	
Name:	Mikko Vepsäläinen
Title:	Research team leader

Contents

1. Introduction

The main stressors causing aging in polymeric materials are temperature, radiation and presence of oxygen. Through the basic oxidative degradation mechanism, these stressors will dissociate and partially oxidize polymer chains, often leading to increased crystallinity and weakening of the amorphous parts of the material, thereby causing ductile materials to turn brittle. To mitigate these effects, antioxidants are normally added to the polymer composition. In an ideal case, antioxidants prevent or significantly slow down oxidative degradation reactions such that the mechanical and, for cables also, electrical properties are maintained. In doing so, antioxidants are however depleted. If the antioxidants are completely or nearly completely consumed, oxidative degradation of the polymer commences without retarding, leading to rapid degradation of the previously mentioned material properties. Since replacement of polymeric components, such as large amounts of cables, is a significant task, it is desirable to know well in advance (several years) when to start planning such a replacement. Antioxidant levels in materials can offer an early clue into the time available before materials start to severely degrade.

Measuring the antioxidant level is possible using DSC to determine the oxidation induction time, OIT. This requires microsampling of material. However, OIT itself does not measure the actual condition of the polymer, and reliance on OIT measurement implicitly assumes that polymer degradation starts only after OIT reaches zero or a near zero value. It is also possible to use similar microsampling to conduct Fourier transform infrared spectroscopy (FTIR) measurements to look for direct evidence of polymer oxidation, such as carbonyl, alcohol or aldehyde groups. These methods are however currently not widely used, and the standard quantity used to characterize the mechanical properties remains elongation at break from a standard tensile test. Comparison of OIT and FTIR measurements has indicated in some cases that oxidation indeed starts when OIT is zero (Salivon et al. 2022) while in other cases oxidation products have been detected while OIT is still non-zero (Celina et al. 2006, Byrne et al. 2020). In particular, the study by Celina et al. (2006) indicated oxidation of polybutadiene with significant phenolic antioxidant levels still measured in the sample. For condition monitoring purposes, understanding these effects would be important.

A complementary approach to experiments is offered by numerical methods to estimate antioxidant consumption. These methods require assumptions on species diffusion and reaction kinetics. A system of ordinary differential equations is then set up that can be solved for example by finite element methods. Such models have been developed especially by ENSAM, France (Rincon-Rubio et al. 2001, Khelidj et al. 2006), and to some extent Sandia National Laboratories, USA (Wise et al. 1997). Equations describing antioxidant consumption have been added to the ENSAM model (Richaud 2013). The ENSAM model without DLO (i.e. assuming oxygen excess) has been tentatively tested at VTT in the SAFIR2022 SAMPO project (Vaari 2021).

The goal of the present work is to initiate the development of numerical modelling beyond the state of the art. The polymer degradation mechanism, oxygen diffusion, and antioxidant depletion will be implemented in both 2D and 3D finite-element models to obtain realistic component-scale predictions on thermal degradation. As a novelty, antioxidant diffusion and evaporation models shall be added, as it has been argued that loss of antioxidant through evaporation or leaching is in most cases more significant than loss due to chemical reactivity (Allen et al. 2010, Xu et al. 2020).

2. Diffusion and solubility

This chapter provides a brief look at literature concerning the diffusivities and solubilities of oxygen and various antioxidants, as well as evaporation (or extraction) of antioxidants, in various polyethylenes. These are required as input parameters to the finite-element model.

2.1 O2 diffusion and solubility

Seguchi and Yamamoto (1986) determined the diffusion and solubility coefficients of oxygen in LDPE, HDPE and various other polymers in the temperature range 283-353 K. The effects of anaerobic and oxidative gamma ray irradiation on these coefficients were also studied. The paper gives the data in numerical form, allowing reproduction of figures. Figure 1 presents an Arrhenius plot of the diffusion coefficient for unirradiated LDPE and HDPE, and for one LDPE sample irradiated under oxidative atmosphere. Irradiation under oxygen thus decreases diffusivity, which can be explained by increased crystallinity, as evidenced by comparison of LDPE and HDPE data.

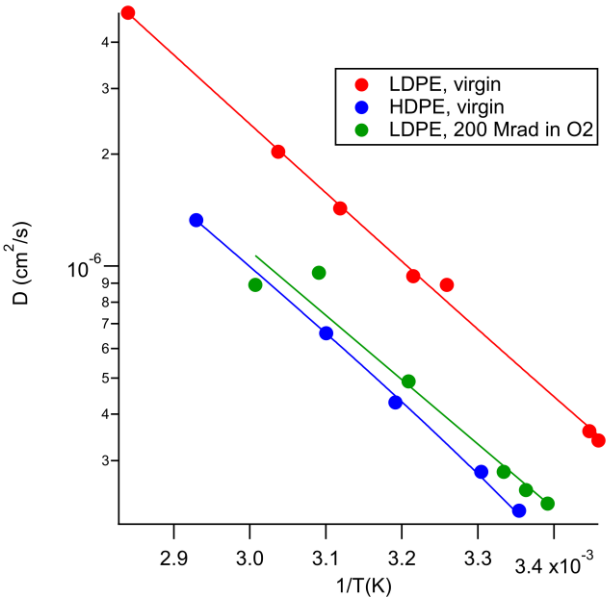

Figure 1. Diffusion coefficient data from Seguchi and Yamamoto (1986).

Writing the diffusion coefficient in the form

$$D = D_0 exp(-E_a/RT)$$

and performing the fits to the data, gives values for D_0 and E_a as shown in Table 1.

Table 1. Arrhenius parameters and values of oxygen diffusion coefficients at selected temperatures according to Seguchi and Yamamoto (1986).

Material	E_a kJ/mol	D_0 m²/s	D@T=30ºC m²/s	D@T=60ºC m²/s
LDPE, virgin	35.2	$8.1 \cdot 10^{-5}$	$6.92 \cdot 10^{-11}$	$2.44 \cdot 10^{-10}$
HDPE, virgin	35.1	$3.2 \cdot 10^{-5}$	$2.84 \cdot 10^{-11}$	$9.98 \cdot 10^{-11}$
LDPE, irradiated	33.1	$1.7 \cdot 10^{-5}$	$3.34 \cdot 10^{-11}$	$1.09 \cdot 10^{-10}$

Villaluenga et al. (1998) examined permeability and diffusivity of oxygen and other gases in LLDPE layer structures in the temperature range 298-358 K. The crystallinities of the material were 24-30%. Data is only shown as Arrhenius plots, from which activation energies of 25.5 - 47.1 kJ/mol were determined by the authors. Values at 298 K for the diffusion coefficients are from $4.7 \cdot 10^{-8}$ cm²/s to $5.1 \cdot 10^{-7}$ cm²/s. A solubility coefficient at 298 K of 0.07 cm³(STP)/cm³/atm was reported for one of the materials.

Hedenqvist et al. (1996) studied permeation of oxygen in linear and branched polyethylenes as a function of crystallinity and molar mass at T=298.2 K. Oxygen solubilities varied between 0.02 and 0.06 cm^3(STP)/cm^3/atm, and diffusivities between $1.42 \cdot 10^{-7}$ and $1.46 \cdot 10^{-6}$ cm^2/s. Solubility in the amorphous phase was found to increase with crystallinity. Pino et al. (2005) measured diffusion, solubility, and permeability of oxygen through various LLDPE and HDPE grades with crystallinities of 32-70% at 295-298 K. Diffusion coefficients varied between $1.9 \cdot 10^{-7}$ cm^2/s and $5.1 \cdot 10^{-7}$ cm^2/s, while solubilities varied between 0.029 and 0.086 cm^3(STP)/cm^3/atm.

2.2 Physical loss of antioxidants

In addition to chemical consumption, antioxidant can be lost from the material through physical processes. This requires that antioxidant can be transported from the bulk of the material to the surface by diffusion. On the surface, loss can occur through leaching or evaporation. However, the antioxidant may also form a separate phase on the surface in a process called blooming. The latter can be advantageous for the material. Loss of antioxidant through evaporation is significant with respect to the protection time offered by antioxidants. It has been argued that in most cases, physical loss can exceed loss by chemical consumption (Boersma 2006). Quantitatively, writing the diffusion equation for antioxidant, and solving it with appropriate boundary conditions at the surface, leads to a solution containing a dimensionless parameter L:

$$L = \frac{lV_0}{SD}$$

where l is the thickness of the film (m), V_0 is the antioxidant volatility (kg/m^2/s), S is the solubility (kg/m^3), and D the diffusion coefficient (m^2/s). It has been found that if L<0.6, loss is controlled by evaporation, and if L>10, loss is controlled by diffusion.

The protection time offered by an antioxidant may be estimated form the empirical correlation proposed by Moisan and Lever (1982):

$$\tau_{prot} \sim ln\left(\frac{S^2}{D}\right).$$

Malik et al. (1995) used this relation to study HALS protection of LDPE and PP. The stabilizers included Tinuvin 770 (M=512 g/mol), and a tetramethylpiperidine derivative with a long hydrocarbon tail (M≈370 g/mol). They assumed a functional form of

$$ln(\tau_{prot}) = exp\left(A + B\ ln\left(\frac{S^2}{D}\right)\right).$$

and measuring the protection time of various stabilizers at 60 ºC. They found that $ln(S^2/D) \approx 40$, $A \approx 1.7$ and $B \approx 7$, with the protection time given in hours.

Möller and Gevert (1994) studied the diffusion of hindered phenol antioxidants in LDPE ($M_w = 1.03 \cdot 10^5$ g/mol, $M_n = 2.22 \cdot 10^4$ g/mol, volume crystallinity 44%) in the temperature range 30 - 60 ºC. The hydrocarbon tail of the antioxidant varied between 1 and 18 carbon atoms, with the longest molecule corresponding to Irganox 1076 (M=711 g/mol). Their results are compiled in Table 2. Comparison with Table 1 shows that oxygen diffusion is over three orders of magnitude faster than that of Irganox 1076.

Table 2. Arrhenius parameters and values of antioxidant diffusion coefficients at selected temperatures according to Möller and Gevert (1994).

Tail length (n)	E_a	D_0	D@T=30ºC	D@T=60ºC

	kJ/mol	m^2/s	m^2/s	m^2/s
0	87.0	63.6	$5.72 \cdot 10^{-14}$	$135 \cdot 10^{-14}$
2	89.6	147	$4.78 \cdot 10^{-14}$	$125 \cdot 10^{-14}$
5	92.0	323	$4.09 \cdot 10^{-14}$	$114 \cdot 10^{-14}$
11	95.5	776	$2.97 \cdot 10^{-14}$	$89.7 \cdot 10^{-14}$
17	104	14800	$1.43 \cdot 10^{-14}$	$66.6 \cdot 10^{-14}$

Xu et al. (2020b) determined a solubility limit of 0.9 wt-% (0.016 mol/l) for primary antioxidant Irganox 1076 in XLPE. Furthermore, Xu et al. (2020a) determine a solubility limit of 0.9 wt-% (0.012 mol/l) for secondary antioxidant Irganox PS802. Both of these studies point out that antioxidants may typically be present in concentrations above the solubility limits. In such cases, the excess antioxidant separates into a crystalline phase either in the bulk or on the surface. When antioxidant is depleted from the dissolved state, the crystalline phase acts as a reservoir, maintaining the concentration in the dissolved phase.

Lundbäck et al. (2006) studied the loss of Santonox R antioxidant (M=359 g/mol) from branched polyethylene. Specifically, they determined the loss rate at polymer boundary, F_0, which is defined by the boundary condition

$$D\left[\frac{\partial C}{\partial x}\right]_{x=0} = F_0 C$$

This condition states that the diffusive flux coming to the surface (from Fick's law) equals the evaporative flux which is proportional to concentration. When temperature was varied between 75 and 90 ºC, antioxidant diffusion coefficient varied between $1.8 \cdot 10^{-12}$ m^2/s and $4.7 \cdot 10^{-12}$ m^2/s, and the loss rate between $9 \cdot 10^{-11}$ m/s and $36 \cdot 10^{-11}$ m/s. For their HALS compounds Malik et al. (1995) used gravimetry to determine volatility values of $2\ldots6 \cdot 10^{-10}$ $kg/m^2/s$ at 60 ºC. Using a LDPE density of 919 kg/m^3, HALS concentration of 0.2 wt-% (1.8 kg/m^3) and volatility $6 \cdot 10^{-10}$ $kg/m^2/s$, a value of $3.3 \cdot 10^{-10}$ m/s can be calculated for their loss rate F_0.

Note that to mitigate the effects of antioxidant migration, it has been proposed that antioxidants could be grafted to the polymers (Malik et al. 1998, Kim et al. 2000).

3. Finite-element model

The basic autoxidation scheme (BAS) for thermal oxidation of rubber and related materials was first reported by Bolland (1946), and it has become the standard way of describing chemistry leading to oxidative degradation of polymers. When combined with a diffusion equation for oxygen, BAS can be used to compute oxidation profiles across the thickness of the sample. Such 1-dimensional calculations have been reported e.g. by researchers from Sandia National Laboratories, US (Gillen et al. 1995, Wise et al. 1997), and ENSAM, France (Rincon-Rubio et al. 2001).

In a previous SAMPO report (Vaari 2021), the BAS, as formulated by ENSAM, was extended to take into account antioxidant consumption, as reported by Richaud et al. (2013). In addition, a term describing radical formation due to ionizing radiation was added to the initiation reaction. However, the model did not consider oxygen diffusion, and it assumed that all oxidative reactions occurred under oxygen excess. In this work, we will abandon these limiting assumptions. Furthermore, we add the option to consider antioxidant evaporation.

While it would be possible to repeat the earlier 1-dimensional calculations by writing an in-house solver, in this work we generalize the solution of the equations to 2 or 3 dimensions by employing the COMSOL multiphysics solver. One advantage of this approach is that 2D or 3D geometries can handle components of varying surface-to-volume ratios, which is particularly relevant for antioxidant evaporation.

3.1 Model description

3.1.1 Basic Autoxidation Scheme

The BAS involves the following net reactions.

Initiation:

- $RH \rightarrow R\cdot + H\cdot$ (1a)
- $\delta ROOH \rightarrow \alpha R\cdot + \beta ROO\cdot$ (1b)

Propagation:

- $R\cdot + O_2 \rightarrow ROO\cdot$ (2)
- $ROO\cdot + RH \rightarrow ROOH + R\cdot$ (3)

Termination:

- $R_1\cdot + R_2\cdot \rightarrow R_1\text{-}R_2 + X$ (4)
- $R_1\cdot + R_2OO\cdot \rightarrow R_1\text{-}O\text{-}O\text{-}R_2 + X$ (5)
- $R_1OO\cdot + R_2OO\cdot \rightarrow R_1\text{-}O\text{-}O\text{-}R_2 + O_2 + X$ (6)

where R stands for a radical, and the dot explicitly denotes an unpaired valence electron. δ, α, and β in equation (1b) are integers. The X in equations (4-6) explicitly denotes a cross-link event. Hydroperoxide decomposition (1b) can be either uni- or bimolecular.In an expanded form, the unimolecular hydroperoxide reaction is

- $ROOH \rightarrow RO\cdot + OH\cdot$
- $HO\cdot + RH \rightarrow R\cdot + H_2O$
- $RO\cdot + RH \rightarrow ROH + R\cdot$
- $RO\cdot \rightarrow R_1{=}O + R_2 + S$
- Balance: $ROOH \rightarrow 2R\cdot + H_2O + (1 - \gamma_{CO})\ ROH + \gamma_{CO}RO + \gamma_s S$

where S denotes chain scission event, and γ_{CO} and γ_s are the yields of the $RO\cdot$ radical decomposition into a carbonyl and chain scission. Similarly, the bimolecular reaction can be expanded as

- $ROOH + ROOH \rightarrow RO\cdot + ROO\cdot + H_2O$
- $RO\cdot + RH \rightarrow ROH + R\cdot$
- $RO\cdot \rightarrow R_1{=}O + R_2 + S$
- Balance: $ROOH + ROOH \rightarrow R\cdot + H_2O + ROO\cdot + (1 - \gamma_{CO})\ ROH + \gamma_{CO}RO + \gamma_s S$

It is seen that the integers of equation (1b) are (δ=1, α=2, β=0) for unimolecular and (δ=2, α=1, β=1) for bimolecular pathways. Termination reaction (6) is expanded as

- $R_1OO\cdot + R_2OO\cdot \rightarrow [R_1\text{-}O\cdot\cdot O\text{-}R_2]_{cage} + O_2$ (6-0)
- $[R_1\text{-}O\cdot\cdot O\text{-}R_2]_{cage} \rightarrow R_1\text{-}O\text{-}O\text{-}R_2 + X$ (6-1)

- $[R_1\text{-}O\cdot\cdot O\text{-}R_2]_{cage} \rightarrow RO + ROH$ (6-2)
- $[R_1\text{-}O\cdot\cdot O\text{-}R_2]_{cage} \rightarrow 2R\cdot + 2(1 - \gamma_{CO})ROH + 2\gamma_{CO}RO + 2\gamma_s S$ (6-3)

which in addition to hydroperoxide formation shows two reaction paths leading to an alcohol and a carboxyl, one of which involves radical formation through chain scissions. Adding antioxidant to the reaction scheme requires two further equations:

- $AH + ROO\cdot \rightarrow A\cdot + ROOH$ (S1)
- $A\cdot + ROO\cdot \rightarrow ROOA$ (S2)

3.1.2 System of differential equations

From the BAS, a set of ordinary differential equations is derived which describes the time evolution of the relevant chemical species:

$$\frac{d[R\cdot]}{dt} = G\cdot 10^{-7}\cdot I + 2k_{1u}[ROOH] + k_{1b}[ROOH]^2 - k_2[O_2][R\cdot] + k_3[ROO\cdot][RH] - 2k_4[R\cdot]^2 - k_5[R\cdot][ROO\cdot] + 2k_{63}[ROOR]_{cage}$$

$$\frac{d[ROO\cdot]}{dt} = k_{1b}[ROOH]^2 + k_2[O_2][R\cdot] - k_3[ROO\cdot][RH] - k_5[R\cdot][ROO\cdot] + 2k_{60}[ROO\cdot]^2 - k_{S1}[ROO\cdot][AH] - k_{S2}[ROO\cdot][R\cdot]$$

$$\frac{d[ROOH]}{dt} = -k_{1u}[ROOH] - 2k_{1b}[ROOH]^2 + k_3[ROO\cdot][RH] + k_{S1}[ROO\cdot][AH]$$

$$\frac{d[ROOR]_{cage}}{dt} = k_{60}[ROO\cdot]^2 - (k_{61} + k_{62} + k_{63})[ROOR]_{cage}$$

$$\frac{d[O_2]}{dt} = \nabla\cdot(D_{O2}\nabla[O_2]) - k_2[O_2][R\cdot] + k_{60}[ROO\cdot]^2$$

$$\frac{d[AH]}{dt} = \nabla\cdot(D_{AH}\nabla[AH]) - k_{S1}[ROO\cdot][AH]$$

$$\frac{d[A\cdot]}{dt} = k_{S1}[ROO\cdot][AH] - k_{S2}[ROO\cdot][A\cdot]$$

which assumes a low degree of oxidation such that the concentration of methyl groups [RH] remains constant at about 60 mol/l. Notice that to add the effects of oxygen and antioxidant diffusion, terms containing the diffusion coefficients are included in the equations for $[O_2]$ and [AH]. The parameters *k* are reaction rate constants, as described in (Vaari 2021).

The initial conditions are the following:

- $[R\cdot]_{t=0} = [ROO\cdot]_{t=0} = [ROOR]_{t=0} = [A\cdot]_{t=0} = 0$
- $[ROOH]_{t=0} = 1\cdot10^{-4}$ mol/l (when no radiation)
- $[O_2]_{t=0} = 3.8\cdot10^{-4}$ mol/l
- $[AH]_{t=0}$ = case-by-case antioxidant concentration (mol/l)

The initial oxygen concentration above corresponds to a typical value for oxygen solubility in polyethylene, as used in (Hettal et al. 2021a) based on the solubility data from Seguchi and Yamamoto (1986). For the case of no radiation, a small initial hydroperoxide concentration must be assumed, as was done already by Bolland (1946). Regarding radiative initiation, the dose rate I should be given in units of Gy/s (J/(kg·s)), while the radiochemical yield G should be given in historical units of radicals formed per 100 eV of absorbed radiation. The approximate prefactor 10^{-7} handles conversion to SI units (units for G are 1/(100 eV) = 1/($1.6\cdot10^{-17}$ J) = 1/($6.022\cdot10^{23}$ mol^{-1} · $1.6\cdot10^{-17}$ J) = $1.038\cdot10^{-7}$ mol/J). However, since the units of [R·] is mol/(m^3·s), the value further needs to be multiplied by the density.

The boundary conditions are the following (**n** is the surface normal vector):

- $\mathbf{n}\cdot\nabla[R\cdot] = \mathbf{n}\cdot\nabla[ROO\cdot] = \mathbf{n}\cdot\nabla[ROOH] = \mathbf{n}\cdot\nabla[ROOR] = \mathbf{n}\cdot\nabla[A\cdot] = 0$
- $[O_2]_{\partial\Omega} = 3.8\cdot10^{-4}$ mol/l
- $\mathbf{n}\cdot D_{AH}\nabla[AH] = F_0[AH]$

which assume no evaporation of species other than antioxidant, a surface oxygen concentration according to maximum solubility, and an antioxidant loss rate of F_0.

Using the solutions of the above equations, it is possible to obtain the carbonyl concentration, and the concentration of chain scission (S) and cross-linking (X) events as follows:

$$\frac{d[C=O]}{dt} = \gamma_{CO}(k_{1u}[ROOH] + k_{1b}[ROOH]^2) + k_{62}[ROOR]_{cage} + \gamma_{CO}2k_{63}[ROOR]_{cage}$$

$$\frac{dS}{dt} = \gamma_S(k_{1u}[ROOH] + k_{1b}[ROOH]^2) + \gamma_S 2k_{63}[ROOR]_{cage}$$

$$\frac{dX}{dt} = \gamma_4 k_4[R\cdot]^2 + \gamma_5 k_5[R\cdot][ROO\cdot] + k_{61}[ROOR]_{cage}$$

It is further possible to estimate the weight-average molecular weight $M_w(t)$ using the values of S(t) and X(t) and applying the relation (Mikdam et al. (2017)):

$$M_w = \frac{2Mw_0}{2 + (S - 4X)Mw_0}$$

3.2 COMSOL implementation

COMSOL offers a set of interfaces for solving a system of partial differential equations (PDE's). In this work, the Coefficient Form PDE interface is employed. With isotropic coefficients, and a dependent variable $\mathbf{u}=[x_1,x_2,\ldots,x_n]^T$, the Coefficient Form PDE reads:

$$e_a\frac{\partial^2\boldsymbol{u}}{\partial t^2} + d_a\frac{\partial\boldsymbol{u}}{\partial t} + \nabla\cdot(-c\nabla\boldsymbol{u} - \alpha\boldsymbol{u} + \gamma) + \beta\cdot\nabla\boldsymbol{u} + a\boldsymbol{u} = f$$

The coefficients are:

- e_a is the mass coefficient
- d_a is a damping coefficient or mass coefficient
- c is the diffusion coefficient
- α is the conservative flux convection coefficient

• β is the convection coefficient

• a is the absorption coefficient

• γ is the conservative flux source term

• f is the source term

For the problem formulated above in 3.1, it is readily seen that $e_a=\alpha=\beta=\gamma=a=0$. The components of **u** are assigned as follows:

- x_1 = [R·]
- x_2 = [ROO·]
- x_3 = [ROOH]
- x_4 = $[ROOR]_{cage}$
- x_5 = $[O_2]$
- x_6 = [AH]
- x_7 = [A·]

Importantly, the source term f can be a function of all components of **u**. Thus, setting the isotropic damping coefficients to 1 (i.e. d_a=diag(1,1,1,1,1,1,1)), and the diffusion coefficients to c=diag(0,0,0,0,c_{55},c_{66},0), with $c_{55}=D_{O2}$ and $C_{66}=D_{AH}$, we can write the system of equations as follows:

$$\frac{dx_1}{dt} = 10^{-7}GI + 2k_{1u}x_3 + k_{1b}x_3^2 - k_2x_1x_5 + k_3x_2K + 2k_{63}x_4 - 2k_4x_1^2 - k_5x_1x_2$$

$$\frac{dx_2}{dt} = k_{1b}x_3^2 + k_2x_1x_5 - k_3x_2K - 2k_{60}x_2^2 - k_{s1}x_2x_6 - k_{s2}x_2x_7 - k_5x_1x_2$$

$$\frac{dx_3}{dt} = -k_{1u}x_3 - 2k_{1b}x_3^2 + k_3x_2K + k_{s1}x_2x_6$$

$$\frac{dx_4}{dt} = 2k_{60}x_2^2 - (k_{61} + k_{62} + k_{63})x_4$$

$$\frac{dx_5}{dt} - \nabla \cdot (c_{55}\nabla x_5) = -k_2x_1x_5 + k_{60}x_2^2$$

$$\frac{dx_6}{dt} - \nabla \cdot (c_{66}\nabla x_6) = -k_{s1}x_2x_6$$

$$\frac{dx_7}{dt} = k_{s1}x_2x_6 - k_{s2}x_2x_7$$

where K=[RH]=60 mol/l, and the source terms f_i are represented by the right-hand side of the equations.

The Coefficient Form PDE interface can simultaneously handle both Dirichlet and Neumann boundary conditions. The Dirichlet boundary condition is appropriate for specifying the oxygen concentration at the domain boundary, while the Neumann boundary condition can be applied for specifying the evaporation rate of the antioxidant.

The numerical problem is stiff, and especially prone to difficulties when concentrations approach zero. COMSOL offers several ways to improve the stability of the solver. First, the solution generally relies on Newton's method, requiring the evaluation of the Jacobian. Since this evaluation is expensive, it is by default carried out "minimally", i. e. not at every timestep. This behaviour can be changed by the user to

"every timestep". Furthermore, it is possible to increase the maximum number of iterations from the default value of 4, to tighten the tolerance factor, and to change the nonlinear method from Constant (Newton) to Automatic (Newton) or Automatic highly nonlinear (Newton).

Further, since physical concentrations cannot be negative, a means is needed to impose constraints to the solution. This is not possible using the default fully coupled approach which tries to solve all equations during a single iteration. However, constraints can be imposed using the segregated solver approach. The drawback will be decreased robustness and increased computational cost.

To improve convergence of the solution in regions of steep gradients, sufficiently tight meshing should be ensured.

3.3 Calculation example

To demonstrate the capabilities of the model, we simulate one aging experiment with silane-crosslinked PE, manufactured as a tape of 0.5 mm thickness. It has a density of 918 kg/m^3, a crystallinity of 42%, a gel fraction of 71%, and it contains a storage antioxidant (Irganox 1076) at a concentration of 0.6 wt-% (Xu et al. 2021). This material was subjected to radiothermal aging under ambient air at T=47 ºC and at a dose rate of 77.8 Gy/h for up to 210 days. At 42 day intervals, samples of material were removed from the aging facility for characterization, which included FTIR to analyze the amount of carbonyl and hydroperoxide species. In addition, tensile tests were conducted mainly to look for Elongation-at-Break. Experimental data related to these quantities has been reported in (Hettal et al. 2021a).

Modelling was performed in two steps. In the first step, the Matlab model developed in (Vaari 2021) was used to perform simulations in conditions of oxygen excess. This was done because the model runs very fast, and it is therefore convenient to investigate the effect of changes in the kinetic parameters on the results. The purpose was to obtain a set of parameters that

- yield sufficiently accurate levels of carbonyl and hydroperoxide species after 210 days
- lead to a steady-state hydroperoxide concentration at around 100 days
- yield enough chain scissions to completely degrade the gel network
- suggest an Elongation-at-Break of 50% around 50 days

The third point relates to the experimental result suggesting an elastic segment concentration of about 0.13 mol/l. If it is approximately assumed that an elastic segment forms whenever a cross-link is formed, and conversely, an elastic segment is removed whenever chain scission occurs, then the result means that at least 0.2 % of the chemical bonds must break. The last point is related to the data compilation by Fayolle et al. (2007) which shows that for polyethylene, a ductile-to-brittle transition occurs when the molecular weight of the material drops to around 50 kg/mol. For the purpose of this work, we therefore assume that EaB of 50% corresponds to Mw = 50 kg/mol.

In the second step, the set of kinetic parameters found in the first step was transferred to the Comsol model, and a 2-dimensional simulation was carried out for a domain measuring 0.5 mm x 2.0 mm. The purpose was to verify that the results are sufficiently close to the Matlab solutions. No exact overlap could be expected since the Matlab model had no oxygen consumption and no antioxidant evaporation.

The set of kinetic parameters used for the simulations is shown in Table 3. It is taken from (Vaari 2021) with three exceptions that are highlighted in red. In addition, a Dirichlet boundary condition specifying an oxygen concentration of $3.8 \cdot 10^{-4}$ mol/l, and a Neumann boundary condition specifying an antioxidant loss rate of $F_0 = 1.0 \cdot 10^{-10}$ m/s were defined.

Table 3. Parameters of the kinetic model. Values differing from those in (Vaari 2021) are highlighted in red.

	Expression	Units
Initiation	$k1u=8.0e12*exp(-140000/(R*T))$ $k1b=1.0e11*exp(-105000/(R*T))$	s^{-1} $l\ mol^{-1}\ s^{-1}$
Propagation	$k2=2.0e8$ $k3=1.5e10*exp(-73000/(R*T))$	$l\ mol^{-1}\ s^{-1}$ $l\ mol^{-1}\ s^{-1}$
Termination	$k4=8.0e11$ $k5=2.3e11$ $k60=4.9e19*exp(-80000/(R*T))$ $k61=2.0e6$ $k62=1.2e5*exp(-5000/(R*T))$ $k63=4.8e9*exp(-17400/(R*T))$	$l\ mol^{-1}\ s^{-1}$ $l\ mol^{-1}\ s^{-1}$ $l\ mol^{-1}\ s^{-1}$ s^{-1} s^{-1} s^{-1}
Antioxidant	$ks1=2.0e16*exp(-86700/(R*T))$ $ks2=5.0e8$	$l\ mol^{-1}\ s^{-1}$ $l\ mol^{-1}\ s^{-1}$
Diffusion	$D_{O2}=3.0e5*exp(-35000/(R*T))$ $D_{AH}=1.48e4*exp(-104000/(R*T))$	$m^2\ s^{-1}$ $m^2\ s^{-1}$
Yield	$\gamma_{CO}=0.25$ $\gamma_S=0.41$ $\gamma_4=0.5$ $\gamma_5=0.011$	

Results from the Matlab and Comsol simulations are shown in Figure 2. For the purpose of comparison, Comsol results are average values over the domain. Detailed distributions of the quantities are shown further below.

In general, it was found that the default kinetic parameters from (Vaari 2021) resulted in too slow kinetics, and parameters needed adjustment to make the kinetics faster. This could be achieved by increasing the rates of initiation (k_{1u}, k_{1b}) and propagation (k_2, k_3) reactions. Especially increasing the propagation rates made the plateau of the hydroperoxide concentration occur earlier. It also significantly increased the hydroperoxide and carbonyl levels. Increasing the initiation rates also increased hydroperoxide and carbonyl concentrations, but in addition affected the amount of chain scissions. For the results of this work, we chose to adjust only k_{1b} and k_2 without a rigorous justification.

After adjusting the reaction rates, the carbonyl concentrations were still twice too high. This could be improved by decreasing the selectivity γ_{CO}. Choosing an appropriate value was problematic given that in recent papers by ENSAM (Mikdam et al. 2017, Hettal et al. 2021a) the selectivity is close to 1, but in an earlier paper (Rincon-Rubio et al. 2001) very low selectivities were given for low temperatures. However, adjusting γ_{CO} does not affect any other quantities. With set of parameters in Table 3, hydroperoxide concentration stabilizes at 100 days, scissions are at 1.3 % after 210 days (Hettal's model predicts 1.4%), and molecuar weight drops to 50 kg/mol in 58 days. Carbonyl concentration is 0.4 mol/l after 210 days, and storage antioxidant is depleted in 20 days.

Overall, a good agreement exists between the models. The biggest discrepancy is in oxygen concentration, as Matlab model assumes no oxygen consumption. There are also clear differences in the predicted scission and crosslink events, leading to somewhat different molecular weight predictions especially at early stages of aging. With Comsol, it was noted that derived quantities from time integration (C=O, S, X, Mw) required that solutions are saved frequently enough for the integration to be accurate. For this work, one solution per day was stored.

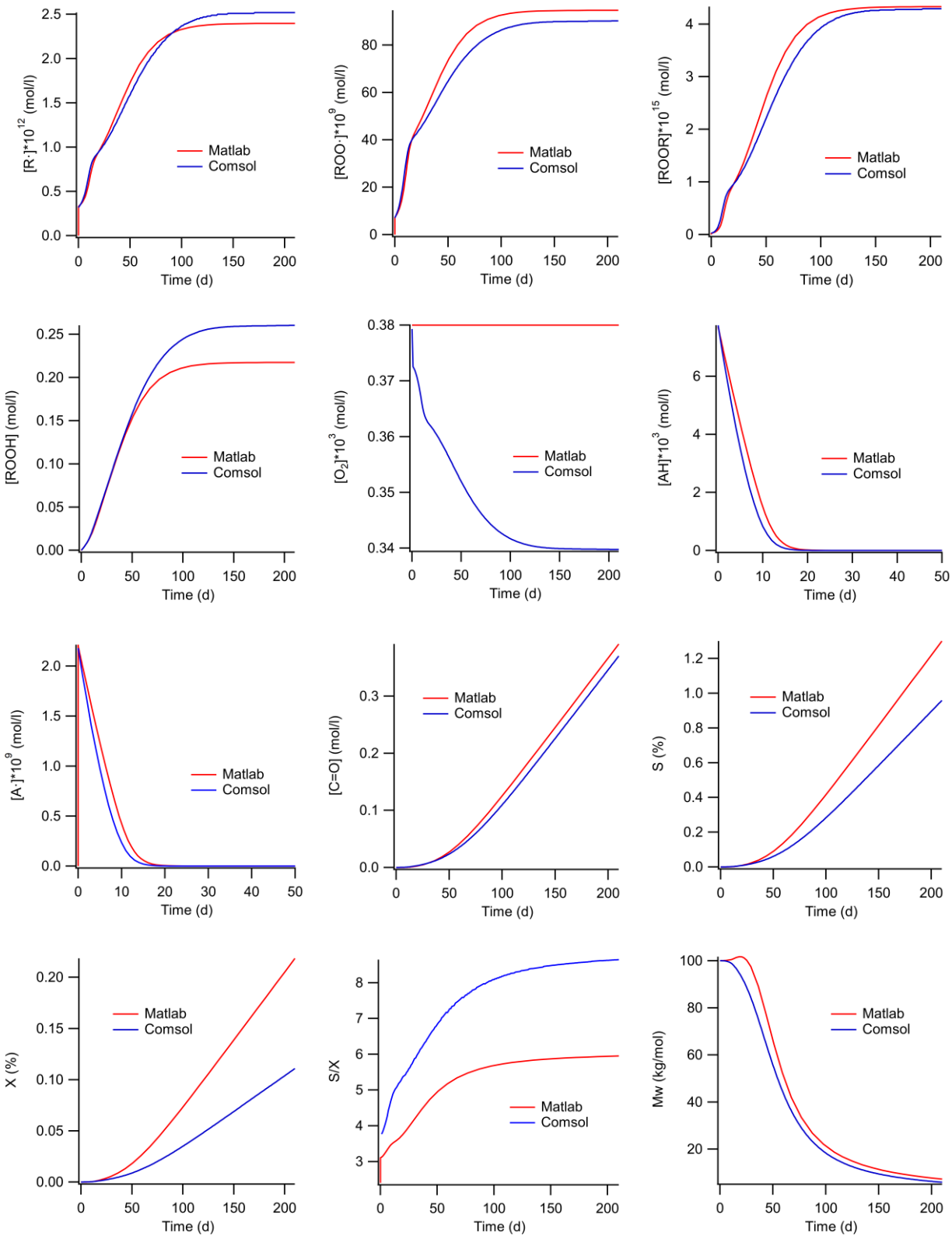

Figure 2. Results from the Matlab and Comsol simulations. S and X are expressed as percentage of the total amount of chemical bonds in the material.

As an example of the 2D solutions available from Comsol, Figure 3 presents the distribution of oxygen concentration at selected times corresponding to sample withdrawals in the aging experiments. Clearly, a concentration gradient develops inside the material during aging. This concentration gradient is the

driving force for oxygen diffusion from the surface deeper into the sample. However, at the center of the material the concentration drops just to 0.31 mol/m^3, which is 81.6% of the surface concentration. This suggests that oxygen diffusion is not severely limiting the aging process for a 0.5 mm thick sample.

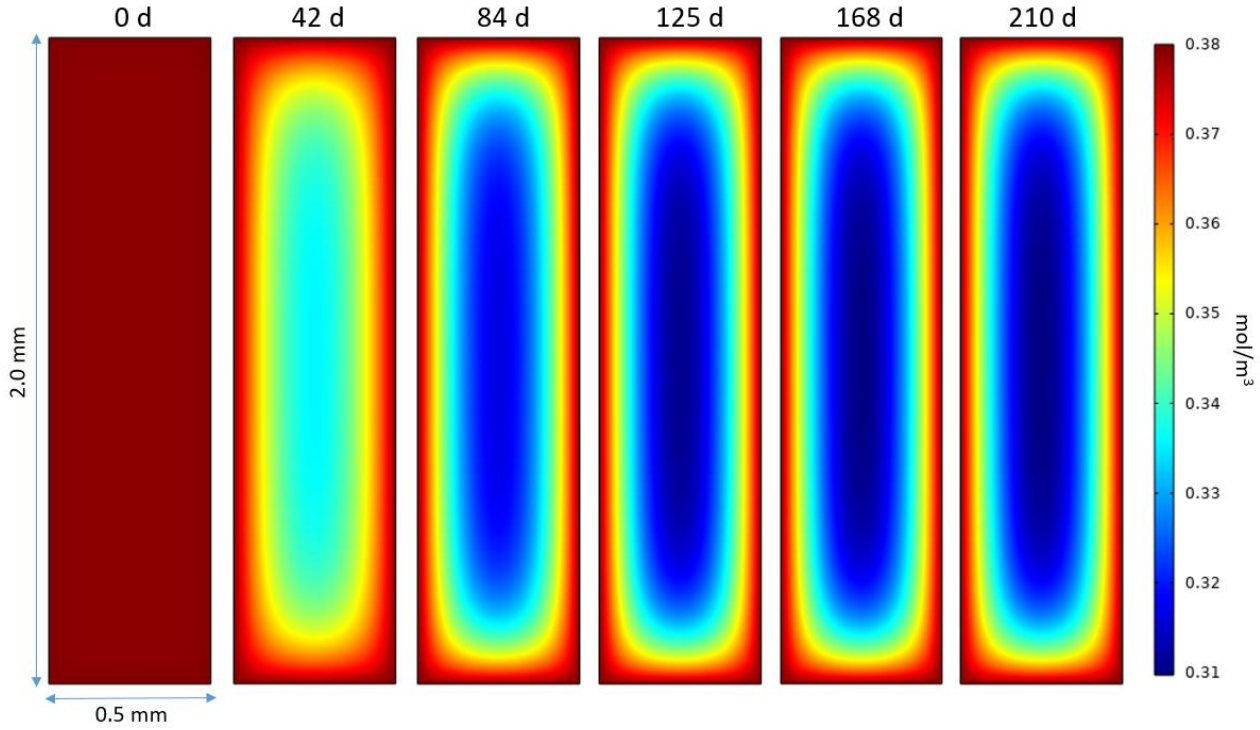

Figure 3. Distribution of oxygen concentration as a function of time for T=47ºC and dose rate 77.8 Gy/h.

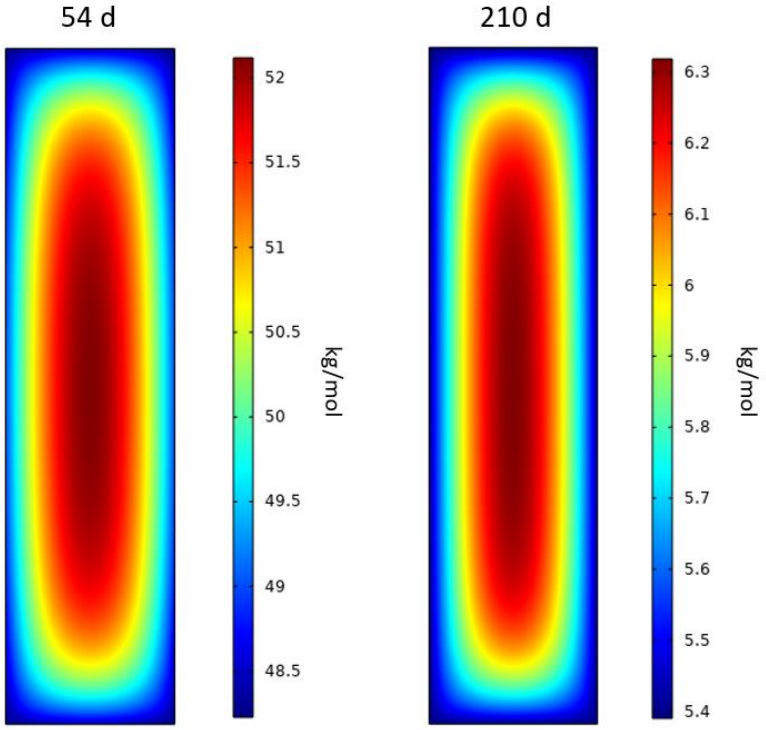

Figure 4. Distribution of molecular weight as a function of time for T=47ºC and dose rate 77.8 Gy/h at t=54 d and t=210 d.

More insight into the potential diffusion limitation of aging is offered by Figure 4 which shows the distribution of molecular weight after 54 and 210 days of aging. The former corresponds to the time at which the molecular weight has dropped from the initial value of 100 kg/mol to 50 kg/mol, corresponding to the ductile-brittle transition. The molecular weight varies modestly, suggesting that the mechanical properties at the surface and in the center of the material do not differ much. The experimental indentation data reported in (Hettal et al. 2022) shows a flat profile for the elastic modulus across sample thickness.

Since the Comsol model includes interaction of the material with environment, the results can be further analyzed to obtain information on the uptake of oxygen and evaporation of antioxidant. Considering first oxygen, we note that oxygen concentration is affected by three processes: uptake (absorption from ambient and subsequent diffusion inside the material), propagation reaction (2) in which a peroxide radical is formed, and interestingly, termination reaction (6) in which two peroxide radicals combine and in which an oxygen molecule is produced, not consumed. In other words, the BAS “recycles” part of the consumed oxygen back to molecular form. The terms corresponding to chemical consumption and regeneration of oxygen can be readily computed separately. To find out the oxygen uptake, we note that

$$\frac{d\langle x_5\rangle}{dt} = -k_2\langle x_1 x_5\rangle + k_{60}\langle x_2^2\rangle + \langle \nabla\cdot(c_{55}\nabla x_5)\rangle$$

where the bracket denotes surface average. The last term can in principle be converted, using the divergence theorem, to a boundary integral which would naturally suggest a Neumann boundary condition for oxygen concentration. However, since it is not possible *a priori* to know the oxygen flux through the boundary, it was decided to apply the simpler Dirichlet boundary condition based on solubility. Regardless of the mathematical finesses, the last term is the oxygen uptake and it can be solved because the other three quantities of the equation are known. The results are plotted in Figure 5. The regeneration rate is non-negligible. The rates assume a steady state after 100 days. At that point, the net oxygen concentration (Figure 2) does not change, but oxidation reactions proceed at a steady-state rate, driven by oxygen uptake.

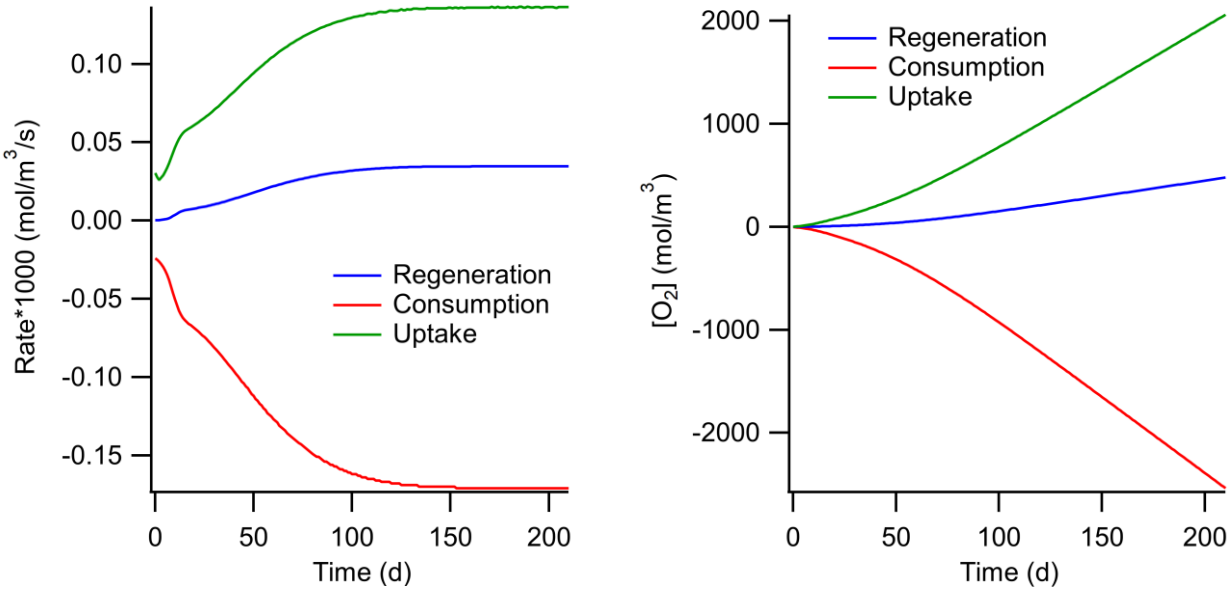

Figure 5. Left: rates of average oxygen uptake, consumption and regeneration processes. Right: the same quantities in time-integrated presentation.

A similar procedure can be applied to the antioxidant. As the antioxidant concentration and rate of chemical consumption are known, the rate of evaporation is readily obtained. Note that an *a priori* flux for

the antioxidant is not know either. In the Neumann boundary condition for antioxidant flux, we only specified a constant of proportionality, loss rate F_0, between surface concentration and evaporative flux. These results are plotted in Figure 6, which shows that evaporation significantly contributes to antioxidant loss, but does not dominate in this case.

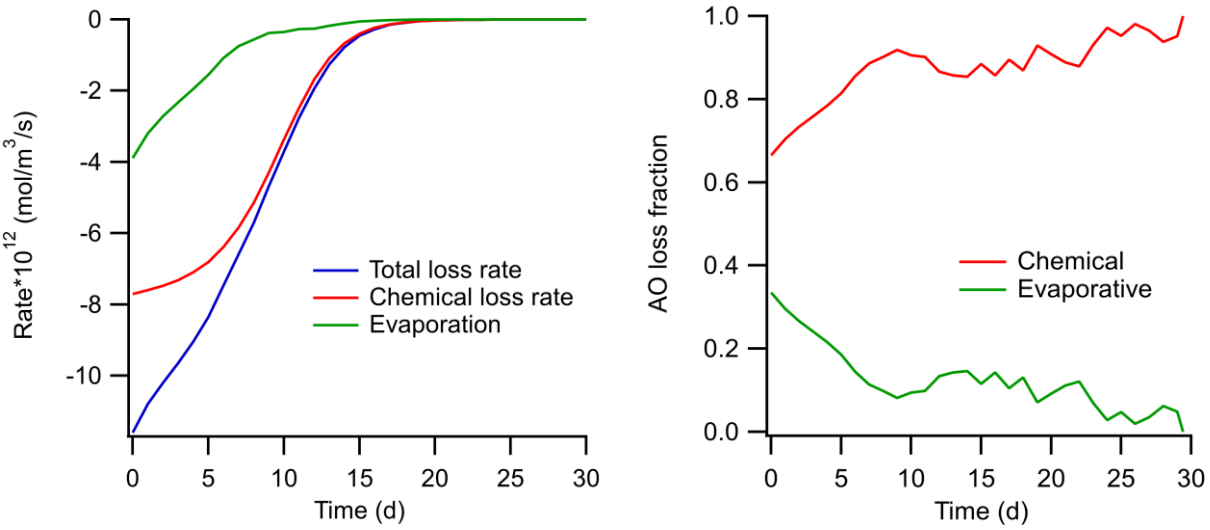

Figure 6. Left: total antioxidant loss rate, and rates of chemical and evaporative loss processes. Right: chemical and evaporative fraction of antioxidant loss rate.

Finally, since oxygen uptake and antioxidant loss rates are known, we might be tempted to estimate the change in the mass of the material based on these quantities. Given an antioxidant loading of 0.6 wt-%, and noting from Figure 6 that about 20 % of this will evaporate, we see that mass change due to antioxidant evaporation is negligible compared to oxygen uptake, which is seen from Figure 7 to be as much as 7% after 210 days.

However, it should be noted that the hydroperoxide decomposition reactions produces water which will evaporate if concentration is above the solubility limit. As evident from the BAS given above in 3.1.1, each hydroperoxide decomposition reaction (either uni- or bimolecular) produces one water molecule. Therefore, for water molecules, we can write

$$\frac{d[H_2O]}{dt} = k_{1u}[ROOH] + 2k_{1b}[ROOH]^2$$

which gives about 1.2 mol/l after 210 days. Data for water solubility in polyethylene can be found e.g. in (McCall et al 1984, Börjesson et al., 2013). Interestingly, Figure 1 of (McCall et al. 1984) indicates that water solubility increases with amount of oxygen bound to the polymer, as oxygenated sites attract water molecules. Still, water solubilities at 298 K are of the order of a few hundred ppm. This means that practically all of the water produced by hydroperoxide decomposition will evaporate.

Figure 7 presents the relative mass change of the material due to oxygen uptake and water evaporation processes. Mass loss due to water evaporation is significant, reducing the net mass change of the material to 4.7 %. There is no experimental data to validate the estimate. For real materials containing a mixture of various additives, mass loss processes can be more complicated. Also, transformation products of chemically consumed antioxidants and even small polymer fragments from chain scissions may evaporate.

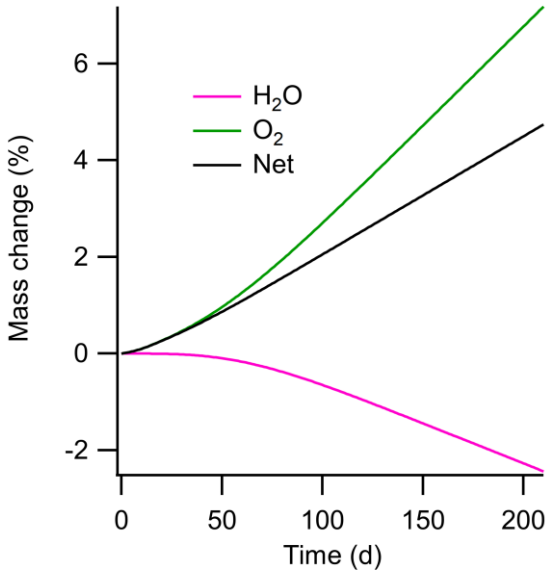

Figure 7. Mass change of the material due to oxygen uptake and water evaporation.

4. Conclusions

In this work, we have initiated the development of numerical antioxidant consumption modelling beyond the state of the art. The polymer degradation mechanism, oxygen diffusion, and antioxidant depletion were implemented in both 2D and 3D finite-element models to obtain realistic component-scale predictions on thermal degradation. As a novelty, antioxidant diffusion and evaporation models were added.

The capabilities of the model were demonstrated by simulating a radiothermal (T=47 ºC, dose rate 77.8 Gy/h) aging of silane-crosslinked, 0.5 mm thick polyethylene up to 210 days. It was shown that the model can reproduce experimentally observed levels of hydroperoxide and carbonyl species, and predict a decrease of the molecular weight of the material such that the cross-linked gel network is completely degraded, and that the mechanical properties of the material are severely compromised.

Several aspects of the model need further work.

The kinetic parameters used in the model are compiled from several papers, and sometimes values for a given parameter differs from one source to another. The origin of the parameters should be better understood, which hopefully would give a better idea on their accuracy and applicability to various materials and aging conditions. The various experimental aging treatments reported in the literature could be systematically employed for validation.

Further derived quantities can be developed. For example, the chain scission and cross-linking rates could be used as inputs for a numerical graph model (Verho and Vaari 2022) in order to get more insight into the molecular-lever structure of the material. It could be envisioned that this way, the gradual changes in the mechanical properties such as elastic modulus, and elongation at break could be modelled in a physical rather than an empirical fashion. On the other hand, since concentration of oxygen-containing groups is known from the model, and their effect on the polarization is known, the dielectric properties can be included in the model, as demonstrated by (Hettal et al. 2021b).

The current work has not attempted to utilize the full power of Comsol to model complex geometries. Thus, extending the modelling to real components such as electrical cables with an internal structure and

several material components could be done in the future. While a cable could be basically handled with a 2D model, it should be possible to develop also 3D models for more complex components. In addition, interaction of the component with environment could be included using the multi-physics capabilities of Comsol, adding for example a non-isotropic heat flux, mimicking a component near a hot spot.

References

Allen, N.S., Zeynalov, E.B., del Teso Sanchez, K., Edge, M., Kabetkina, Y.P., Johnson, B. 2010. Comparative evaluation of the efficiency of a series of commercial antioxidants studied by kinetic modeling in a liquid phase and during the melt processing of different polyethylenes. Vinyl & Additive Technology 16, 1-14. https://doi.org/10.1002/vnl.20208

Boersma, A. 2006. Predicting the efficiency of antioxidants in polymers. Polymer Degradation and Stability 91, 472-478. https://doi.org/10.1016/j.polymdegradstab.2005.08.007

Bolland, J.L. 1946. Kinetic studies in the chemistry of rubber and related materials. I. The thermal oxidation of ethyl linoleate. Proceedings of the Royal Society A 186, 218-236. https://doi.org/10.1098/rspa.1946.0040

Byrne, N., De Silva, R., Hilditch, T. 2020. Linking Antioxidant Depletion with Material Properties for Polyethylene Pipes Resins. Polymer Engineering and Science 60, 323-329. https://doi.org/10.1002/pen.25287

Börjesson, A., Erdtman, E., Ahlstrom, P., Berlin, M., Andersson, T., Bolton, K. 2013. Molecular modelling of oxygen and water permeation in polyethylene. Polymer 54, 2988-2998. https://doi.org/10.1016/j.polymer.2013.03.065

Celina, M., Skutnik Elliott, J.M., Winters, S.T., Assink, R.A., minier, L.M. 2006. Correlation of antioxidant depletion and mechanical performance during thermal degradation of an HTPB elastomer. Polymer Degradation and Stability 91, 1870-1879. https://doi.org/10.1016/j.polymdegradstab.2005.11.006

Fayolle, B., Colin, X., Audouin, L., Verdu, J. 2007. Mechanism of degradation induced embrittlement in polyethylene. Polymer Degradation and Stability 92, 231-238. https://doi.org/10.1016/j.polymdegradstab.2006.11.012

Gillen, K.T., Wise, J., Clough, R.L. 1995. General solution for the basic autoxidation scheme. Polymer Degradation and Stability 47, 149-161. https://doi.org/10.1016/0141-3910(94)00105-H

Hedenqvist, M., Angelstok, A., Edsberg, L., Larsson, P.T., Gedde, U.W. 1996. Diffusion of small-molecule penetrants in polyethylene: free volume and morphology. Polymer 37, 2887-2902. https://doi.org/10.1016/0032-3861(96)89384-0

Hettal, S., Roland, S., Sipilä, K., Joki, H., Colin, X. 2021a. A new analytical model for predicting the radio-thermal oxidation kinetics and the lifetime of electric cable insulation in nuclear power plants. application to silane cross-linked polyethylene. Polymer Degradation and Stability 185, 109492. https://doi.org/10.1016/j.polymdegradstab.2021.109492

Hettal, S., Suraci, S.V., Roland, S., Fabiani, D., Colin, X. 2021b. Towards a Kinetic Modeling of the Changes in the Electrical Properties of Cable Insulation during Radio-Thermal Ageing in Nuclear Power Plants. Application to Silane-Crosslinked Polyethylene. Polymers 13, 4427. https://doi.org/10.3390/polym13244427

Hettal, S., Roland, S., Colin, X. 2022. Consequences of Radiothermal Ageing on the Crystalline Morphology of Additive-Free Silane-Crosslinked Polyethylene. Polymers 14, 2912. https://doi.org/10.3390/polym14142912

Khelidj, N., Colin, X., Audouin, L., Verdu, J., Monchy-Leroy, C., Prunier, V. 2006. Oxidation of polyethylene under irradiation at low temperature and low dose rate. Part II. Low temperature thermal oxidation. Polymer Degradation and Stability 91,1598-1605. https://doi.org/10.1016/j.polymdegradstab.2005.09.012

Kim et al 2000 https://doi.org/10.1002/1097-4628(20000923)77:13%3C2968::AID-APP21%3E3.0.CO;2-T

Lundbäck, M., Strandberg, C., Albertsson, A.-C., Hedenqvist, M.S., Gedde, U.W. 2006. Loss of stability by migration and chemical reaction of Santonox® R in branched polyethylene under anaerobic and aerobic conditions. Polymer Degradation and Stability 91, 1071-1078. https://doi.org/10.1016/j.polymdegradstab.2005.07.010

Malik, J., Tuan, D.Q., Spirk, E.1995. Lifetime prediction for HALS-stabilized LDPE and PP. Polymer Degradation and Stability 47, 1-8. https://doi.org/10.1016/0141-3910(94)00098-S

Malik, J., Ligner, G., Avar, L. 1998. Polymer bound HALS - expectations and possibilities. Polymer Degradation and Stability 60, 205-213. https://doi.org/10.1016/S0141-3910(97)00082-7

McCall, D.W., Dougless, D.C., Blyler Jr, L.L., Johnson, G.E., Jelinski, L.W., Bair, H.E. 1984. Solubility and Diffusion of Water in Low-Density Polyethylene. Macromolecules 17, 1644-1649. https://pubs.acs.org/doi/pdf/10.1021/ma00139a001

Mikdam, A., Colin, X., Minard, G., Billon, N., Maurin, R. 2017. A kinetic model for predicting the oxidative degradation of additive free polyethylene in bleach desinfected water. Polymer Degradation and Stability 146, 78-94. https://doi.org/10.1016/j.polymdegradstab.2017.09.020

Moisan, J.Y., Lever, R. 1982. Diffusion des additifs du polyethylene—V: Influence sur le vieillissement du polymere. European Polymer Journal 18, 407-411. https://doi.org/10.1016/0014-3057(82)90177-X

Möller, K., Gevert, T. 1994. An FTIR solid-state analysis of the diffusion of hindered phenols in low-density polyethylene (LDPE): The effect of molecular size on the diffusion coefficient. Journal of Applied Polymer Science 51, 895-903. https://doi.org/10.1002/app.1994.070510512

Richaud, E. 2013. Kinetic modelling of phenols consumption during polyethylene thermal oxidation. European Polymer Journal 49, 2223-2232. http://dx.doi.org/10.1016/j.eurpolymj.2013.04.027

Rincon-Rubio, L.M., Fayolle, B., Audouin, L., Verdu, J. 2001. A general solution of the closed-loop kinetic scheme for the thermal oxidation of polypropylene. Polymer Degradation and Stability 74, 177–188. https://doi.org/10.1016/S0141-3910(01)00154-9

Salivon, T., Comte, R., Colin, X. 2022. Thermal aging of electrical cable insulation made of cross-linked low density polyethylene for under-hood application in automotive industry. Journal of Vinyl & Additive Technology 28, 418-429. https://doi.org/10.1002/vnl.21916

Seguchi, T., Yamamoto, Y. 1986. Diffusion and Solubility of Oxygen in γ-ray Irradiated Polymer Insulation Materials. Japan Atomic Energy Research Institute JAERI report 1299. https://inis.iaea.org/collection/NCLCollectionStore/_Public/18/008/18008584.pdf

Vaari, J. 2021. Reaction kinetics of antioxidants for polyolefins. VTT Research Report VTT-R-01051-21.

Verho, T., Vaari, J. 2022. Analytical and Numerical Modeling of Degradation and Pyrolysis of Polyethylene: Measuring Aging with Thermogravimetry. Polymers 14, 2709. https://doi.org/10.3390/polym14132709

Villaluenga, J.P.G., Seoane, B., Compan, V. 1998. Diffusional characteristics of coextruded linear low-density polyethylenes prepared from different conditions of processing. Journal of Applied Polymer Science 70, 23-37. https://doi.org/10.1002/(SICI)1097-4628(19981003)70:1%3C23::AID-APP5%3E3.0.CO;2-W

Wise, J., Gillen, K.T., Clough, R.L. 1997. Quantitative model for the time development of diffusion-limited oxidation profiles. Polymer 38, 1929-1944. https://doi.org/10.1016/S0032-3861(96)00716-1

Xu, A., Roland, S., Colin, X. 2020a. Thermal ageing of a silane-crosslinked polyethylene stabilised with a thiodipropionate antioxidant. Polymer Degradation and Stability 181, 109276. https://doi.org/10.1016/j.polymdegradstab.2020.109276

Xu, A., Roland, S., Colin, X. 2020b. Physico-chemical characterization of the blooming of Irganox 1076® antioxidant onto the surface of a silane-crosslinked polyethylene blooming. Polymer Degradation and Stability 171, 109406. https://doi.org/10.1016/j.polymdegradstab.2019.109046

Xu, A., Roland, S., Colin, X. 2021. Thermal ageing of a silane-crosslinked polyethylene stabilised with an excess of Irganox 1076®. Polymer Degradation and Stability 189, 109597. https://doi.org/10.1016/j.polymdegradstab.2021.109597